Available online at www.sciencedirect.com

ScienceDirect

Ceramics International 40 (2014) 4617–4621

CERAMICS INTERNATIONAL

www.elsevier.com/locate/ceramint

Effects of sintering temperature on the properties of donor-acceptor codoped $Ba_{0.67}Sr_{0.33}TiO_3$ ceramics for pyroelectric infrared detector applications

Zunping Xu[a,*], Hua Qiang[b], Yi Chen[a], Chaoyin Nie[a]

[a]College of Materials Science and Engineering, Southwest University, Chongqing 400715, China
[b]College of Humanistic and Technology of Chongqing, Chongqing 400715, China

Received 14 July 2013; received in revised form 31 August 2013; accepted 31 August 2013
Available online 7 September 2013

Abstract

$Ba_{0.67-x}Y_xSr_{0.33}Ti_{1-y}Mn_yO_3$ [(Mn+Y: BST), $x=0.006$, $y=0.005$] ceramics were fabricated via using citrate–nitrate combustion derived powder, and their microstructure, dielectric properties and pyroelectric properties were systemically investigated within sintering temperature ranged from 1200 °C to 1310 °C. Slight agglomerated BST powders, with nano-size parties, were produced at calcining temperature of 800 °C. Sintering temperature has a great influence on the microstructure and electrical properties of the ceramic samples. The dielectric and pyroelectric properties are improved with sintering temperature increased from 1200 °C to 1280 °C. At room temperature, the Mn+Y: BST ceramics sintered at 1280 °C for 3 h exhibit optimal electrical properties: dielectric loss tan $\delta=0.007$, intrinsic pyroelectric coefficient $\gamma=773$ nC/cm^2 K and figure-of-merit $F_D=134.5$ μPa$^{-0.5}$ at 100 Hz, respectively. Improvement of pyroelectric properties is beneficial to the development of infrared detectors.

Keywords: A. Sintering; C. Dielectric properties; D. Perovskites

1. Introduction

In the past decades, much attention had been paid to the pyroelectric detection of infrared radiation (IR) due to the advantages offered by the pyroelectric detectors: room temperature operation, good sensitivity, and flat spectral response from near ultraviolet up to far infrared [1–5]. In view of pyroelectric infrared detector applications, a good pyroelectric material needs to have higher pyroelectric coefficient, mezzo dielectric constant and lower dielectric loss. Barium strontium titanate (BST) is becoming one of the most interesting pyroelectric materials for uncooled infrared detectors due to its relatively high pyroelectric coefficient. Nevertheless, it is extremely difficult to obtain the pure BST ceramics with good pyroelectric properties. For many years, doping has been used to modify the electrical properties of BST ceramics. As reported, the codoping is an effective way to optimize the electrical properties of $Ba_{1-x}Sr_xTiO_3$ ceramics [6].

As well-known, dielectric properties, based on phase transition phenomena in ferroelectric materials, are closely related to crystal structure. On the other hand, crystal structure of ferroelectric material depends on the thermal history and the fabrication method [7]. Thus, improving the sinterability of BST materials appears as an intriguing subject of practical importance. It was reported that superfine BST powders with high reactivity can be prepared by the citrate precursor method [8,9], which improved sinterability and enhanced electrical properties of BST ceramics [10]. However, this method involves too complex processes and the powders obtained were always badly agglomerated.

In this paper, we present a simple citrate–nitrate combustion method for the synthesis of nanocrystalline $Ba_{0.67-x}Y_xSr_{0.33}Ti_{1-y}Mn_yO_3$ (Mn+Y: BST) powders. A systematic study of effects of sintering temperature on the microstructure, dielectric and pyroelectric properties of the obtained Mn+Y: BST ceramics were investigated.

*Corresponding author. Tel.: +86 023 68251046; fax: +86 023 68254373.
E-mail address: xzp16213@163.com (Z. Xu).

0272-8842/$ - see front matter © 2013 Elsevier Ltd and Techna Group S.r.l. All rights reserved.
http://dx.doi.org/10.1016/j.ceramint.2013.08.139

2. Experimental

The powders of $Ba_{0.67-x}Y_xSr_{0.33}Ti_{1-y}Mn_yO_3$ ($x=0.006$, $y=0.005$) were synthesized by the citrate precursor method. Required amount of barium nitrate, strontium nitrate, tetrabutyl titanate and additions (manganese acetate, yttrium oxide) were dissolved into citrate solution to prepare the precursor solution. Ethylene glycol and glacial acetic acid were used as dispersant and solvents of tetrabutyl titanate, respectively, and an appreciate amount of aqueous ammonia was dripped to adjust pH value of the solution to 6–7. This solution was put into a beaker and the beaker was immersed in a basin with hot silicon oil (80 °C) and then the solution was stirred for 4–6 h, lastly a transparent precursor solution was obtained. The precursor solution was subjected to heating in an oven at 200 °C to form a porous and black solid mass, and then calcined at 800 °C for 3 h in air. The calcined powders were uniaxially pressed into discs, and sintered into ceramics at 1200–1310 °C for 3 h in air.

The density of the ceramic samples was measured by the Archimedes method. The shrinkage of samples was determined by $S=(D_g-D_s/D_g)100\%$, where S is shrinkage, D_g and D_s are the diameters of green body and sintered samples respectively. The crystal structures of the sintered ceramics were confirmed by X-ray diffraction (XRD, DX-1000, Dandong, China). The microstructure of the specimens was observed by scanning electron microscopy (SEM, Inspect F, FEI Company, Netherlands). The dielectric properties as a function of temperature were measured using precision LCR meter (E4980A). The polarization versus electric field (P–E) hysteresis loops were measured by using Radiant Precision Ferroelectric Measurement System (RT2000 Tester, USA).

3. Results and discussion

Fig. 1 shows the SEM observation of calcined Mn+Y: BST powders. As shown in Fig. 1, homogeneous and spongy agglomerations composed of fine preliminary particles of ~100 nm can be seen for the powders.

Fig. 2 shows the X-ray diffraction patterns of Mn+Y: BST ceramics sintered at 1200–1310 °C for 3 h. As shown in Fig. 2,

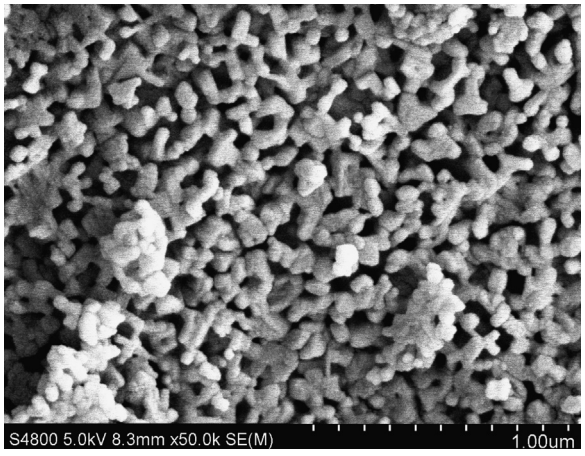

Fig. 1. SEM observation of the calcined Mn+Y: BST powders.

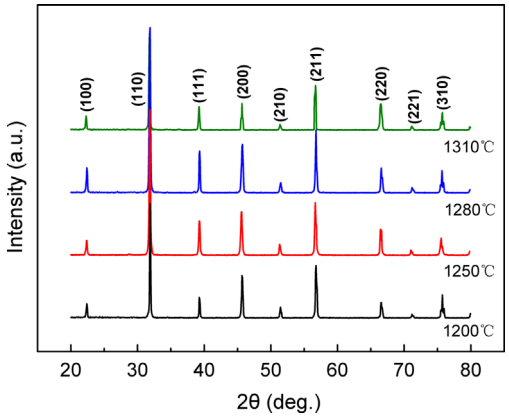

Fig. 2. XRD patterns of Mn+Y: BST ceramics sintered at 1200–1310 °C for 3 h.

all ceramic specimens exhibit a pure perovskite phase and no secondary phase can be detected within the detection limit of X-ray diffraction pattern, indicating that the additions of Mn and Y are dissolved into the BST perovskite lattice. The intensities of diffraction peak, such as (110), (111) and (200) increased with sintering temperature increased from 1200 °C to 1280 °C. It was due to the improved crystallinity of the specimen. This also can be seen in Fig. 3. Further increasing the sintering temperature would lead to a deteriorative crystallization state of ceramic samples. These results suggest that sintering temperature has significant influence on crystallization of the Mn+Y: BST ceramics.

Fig. 3 presents the microstructures of the ceramic specimens that were sintered at different temperatures for 3 h. As shown in Fig. 3, the specimen sintered at 1200 °C has a porous microstructure with fine grains. The grain size of the ceramic samples increased and porosity decreased with the sintering temperature increased from 1200 °C to 1280 °C. An abnormal grain growth was noticed for the ceramic specimen that was sintered at 1310 °C. Mn+Y: BST ceramics have a larger grain size and more closed packed structure than the pure BST ceramics [11]. It was believed that the introduction of Mn and Y additions to BST would decrease the sintering activation energy and reduce the sintering temperature of BST ceramics, and thus enhanced crystallization of ceramic samples.

Fig. 4 shows the relative density and shrinkage of Mn+Y: BST ceramics. Archimedean method was used for bulk densities measurements, and relative densities were calculated as percentages of measured density compared to theoretical density. The relative bulk density and shrinkage increased with increasing sintering temperature to 1280 °C, and then decreased when further increasing sintering temperature to 1310 °C. The specimen sintered at 1280 °C for 3 h has the highest relative density of 98.2% and shrinkage of 17.1%. It may be due to the uniformity grain growth and closed packed microstructure.

Fig. 5. displays the P–E hysteresis loops measured at room temperature for Mn+Y: BST ceramics sintered at different temperatures. For the ceramic specimen sintered at 1200 °C showed a weak remanent polarization (P_r). This was

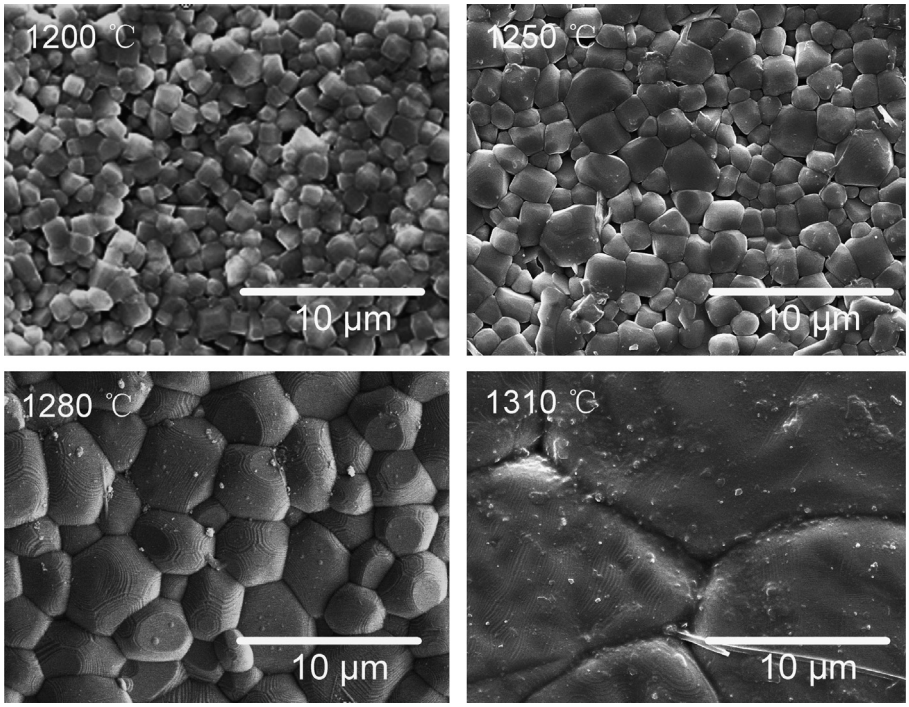

Fig. 3. Microstructure of Mn+Y: BST ceramics sintered at 1200–1310 °C for 3 h.

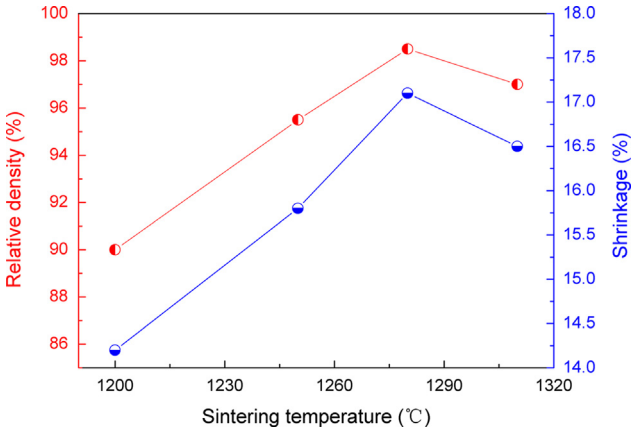

Fig. 4. Relative density and shrinkage of Mn+Y: BST ceramics sintered at 1200–1310 °C for 3 h.

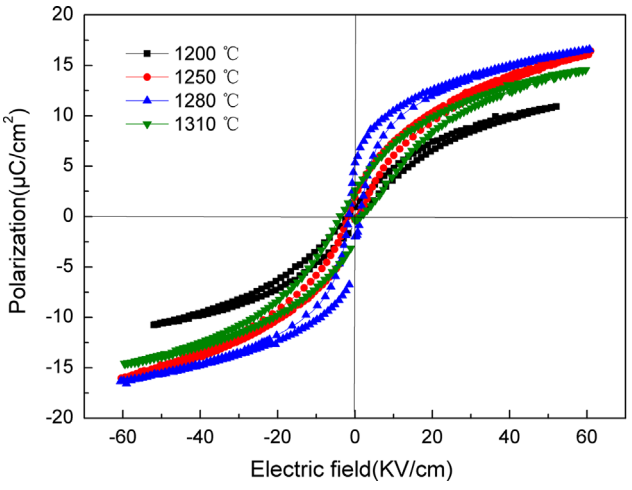

Fig. 5. *P–E* hysteresis loops for Mn+Y: BST ceramics sintered at different temperatures.

presumably due to the porous microstructure and lower density of the specimen. The P_r of ceramic samples increased with increasing sintering temperature, and reached a maximum value of 6.5 μC/cm^2 at the sintering temperature of 1280 °C. This was ascribed to the larger grains of the specimen sintered at higher temperature, which was favorable to the development of the polar micro-regions in size and/or volume fraction [12]. As the grain size distribution became normal grain distribution, the number of domains increased and the spontaneous polarization also increased [13]. However, further increasing the sintering temperature to 1310 °C weakened the ferroelectric properties of the Mn+Y: BST ceramics. It might be due to the lower density and deteriorative crystallization state of the specimen.

Fig. 6 shows the temperature dependence of dielectric constant and loss for Mn+Y: BST ceramics sintered at different temperatures. The Curie temperature (T_C) decreased from 28 °C to 25 °C and dielectric constant peak increased from 5943 to 11296 when the sintering temperature increased from 1200 °C to 1280 °C, respectively. The Curie temperature of Mn+Y: BST ceramics decreased with increasing the sintering temperature, due to the decreasing porosity [14]. The dielectric constant of Mn+Y: BST ceramics increased with increasing the sintering temperature, it was due to the dense microstructure and large grain size of the ceramic samples. The dielectric loss of Mn+Y: BST ceramics sintered

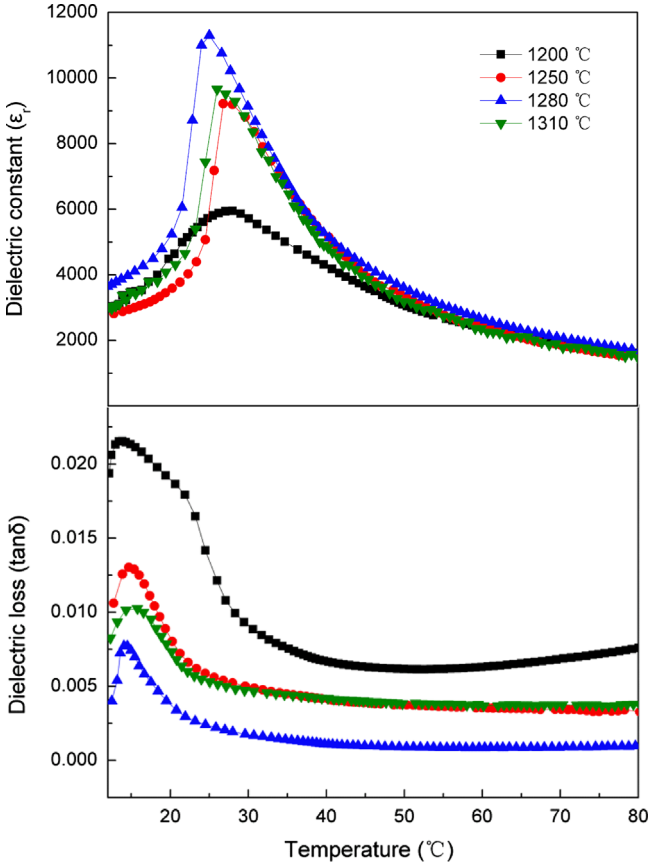

Fig. 6. Temperature dependence of dielectric constant and loss for Mn+Y: BST ceramics sintered at 1200–1310 °C for 3 h at 10 kHz.

at 1280 °C attained the minimum value, which was much lower in the paraelectric state (~0.0025) than in the ferroelectric state (~0.0076), owning to the disappearance of domain. The dielectric loss of all the ceramic samples was significantly reduced with respect to the un-doped ones [11]. It is widely accepted that the electrons resulting from the generation of oxygen vacancy that formed during the sintering process in atmospheres of low oxygen contents can hop between different titanium ions inducing the reduction of Ti^{4+} to Ti^{3+}, which provides a mechanism for dielectric losses. Just as follows:

$$O_O \rightarrow V_O^{\cdot\cdot} + \frac{1}{2}O_2\uparrow + 2e' \quad (1)$$

The incorporation of Mn^{2+} to Ti^{4+} sites can be expresses by the following point defect reaction.

$$MnO + AO \xrightarrow{ABO_3} Mn_B^{''} + A_A + 2O_O + V_O^{\cdot\cdot} \quad (2)$$

When Mn^{2+} ions substitute Ti^{4+} in the BST lattice, oxygen vacancies ($V_O^{\cdot\cdot}$) were created in order to maintain the charge balance, which could decrease the concentration of the electrons, and prevent the reduction of Ti^{4+} to Ti^{3+}.

When Y^{3+} ions substitute Ba^{2+} in the BST lattice, the cation vacancy was induced, which could suppress the creation of $V_O^{\cdot\cdot}$. Just as follows:

$$Y_2O_3 + 3BO_2 \xrightarrow{ABO_3} 2Y_A^{\cdot} + 3B_B + 9O_O + V_A^{''} \quad (3)$$

Consequently, a lower carrier concentration was obtained in the Mn+Y: BST ceramics and thus promoted lower dielectric losses.

The pyroelectric coefficient can be expresses as [15]:

$$\gamma = \frac{dP}{dT} + \varepsilon_0 \int_0^E \left(\frac{d\varepsilon_r}{dT}\right) dE \quad (4)$$

where P is the polarization, T the temperature, E the bias field, and ε_r is the dielectric constant. According to Eq. (4), the total pyroelectric coefficient (γ) consists of the intrinsic pyroelectric coefficient (spontaneous polarization contribution) and the field induced pyroelectric coefficient (the dielectric contribution). Fig. 7(a) displays the intrinsic pyroelectric coefficient for Mn+Y: BST ceramics sintered at different temperatures. As shown in Fig. 7(a), sintering temperature has a strong effect on the intrinsic pyroelectric coefficient of Mn+Y: BST ceramics. The intrinsic pyroelectric coefficient increased from 300 to 773 nC/cm^2 K when the sintering temperature increased from 1200 °C to 1280 °C, and then decreased to 554 nC/cm^2 K when further increasing the sintering temperature to 1310 °C. As the specimen has low porosity [14] and normal grain size distribution [13], there is a high pyroelectric coefficient. For BST materials, the dielectric constant changes significantly

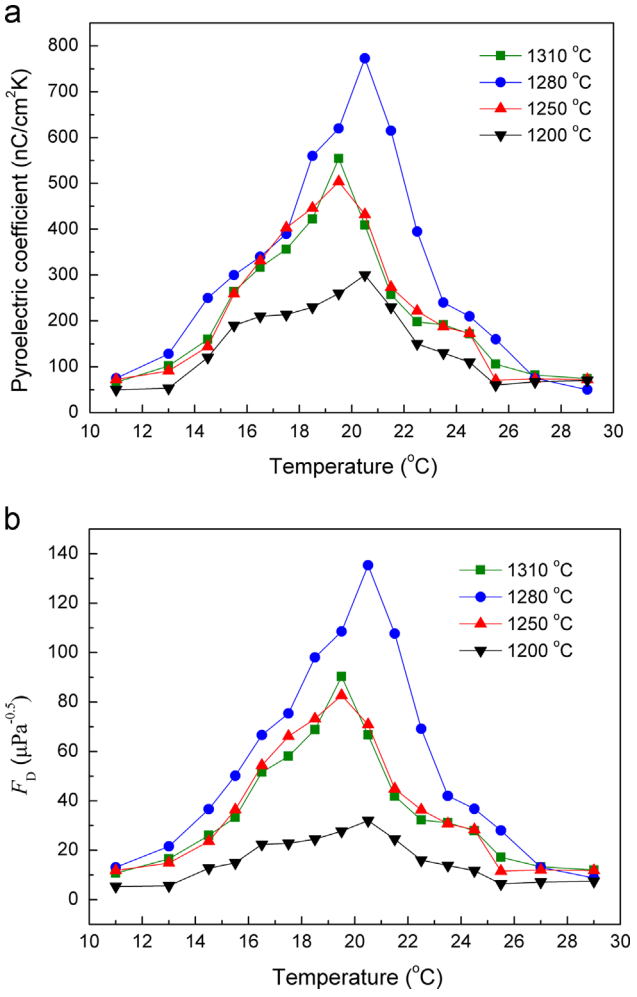

Fig. 7. Temperature dependence of (a) pyroelectric coefficient and (b) figure-of-merit of Mn+Y: BST ceramics sintered at 1200–1310 °C for 3 h at 100 Hz.

when the ferroelectric–paraelectric phase transition takes place, and thus a large pyroelectric coefficient is to be obtained. For the field induced pyroelectric coefficient of the ceramic samples will be studied in detail in the future.

For uncooled infrared detectors, the figure-of-merit is an important parameter to evaluate the quality of pyroelectric materials [14]. To achieve a better response, it is necessary to increase the pyroelectric figure-of-merit, which requires a combination of such properties as high pyroelectric coefficient, low dielectric constant and losses. The figure-of-merit can be expresses as follows [16]:

$$F_D = \gamma/(C_V\sqrt{\varepsilon_0\varepsilon_r \tan \delta}) \quad (5)$$

here F_D is detectivity, C_V is volume specific heat, ε_0 is the permittivity of free space ($=8.85\times10^{-12}$ F/m), $\tan\delta$ is dielectric loss.

Fig. 7(b) shows the F_D of Mn+Y: BST ceramics sintered at different temperatures. The F_D increased when the sintering temperature increased from 1200 °C to 1280 °C. The specimen sintering at 1280 °C showed a maximum F_D value of 134.5 $\mu Pa^{-0.5}$, due to its high pyroelectric coefficient and low dielectric loss.

4. Conclusion

Mn+Y: BST ceramics were fabricated by using citrate–nitrate combustion derived powder, and their dielectric properties and pyroelectric properties were investigated. Sintering temperatures have been found to have a great effect on the electrical properties of the BST ceramic samples. In general, the dielectric and pyroelectric properties enhance with increasing the sintering temperature to 1280 °C. At room temperature, the ceramic specimen sintered at 1280 °C for 3 h exhibits the optimal properties: $\varepsilon_r=5236$, $\tan\delta=0.007$, $\gamma=773$ nC/cm^2 K and $F_D=134.5$ $\mu Pa^{-1/2}$ at 100 Hz, respectively.

Acknowledgments

This work was supported by the Fundamental Research Funds for the Central Universities (XDJK2013C055).

References

[1] R.W. Whatmore, Pyroelectric ceramics and devices for thermal infrared detection and imaging, Ferroelectrics 118 (1991) 241–259.
[2] M. Noda, K. Inoue, M. Ogura, H.P. Xu, An uncooled infrared sensor of dielectric bolometer mode using a new detection technique of operation bias voltage, Sensors and Actuators A 97–98 (2002) 329–336.
[3] S. Liu, M. Liu, Y. Zeng, C. Li, Preparation and characterization of $Ba_{1-x}Sr_xTiO_3$ thin film for uncooled infrared focal plane arrays, Materials Science and Engineering C 22 (2002) 73–77.
[4] H.J. Noh, S.G. Lee, S.P. Nam, Y.H. Lee, Pyroelectric Properties of arrayed $BaTiO_3$ system thick film for uncooled IR detector, Materials Research Bulletin 45 (2010) 339–342.
[5] M. Noda, K. Hashimoto, T. Kiyomoto, H. Tanaka, A new type of dielectric bolometer mode of detector pixel using ferroelectric thin film capacitors for infrared image sensor, Sensors and Actuators A 77 (1999) 39–44.
[6] D.X. Yan, Z.P. Xu, X.L. Chen, D.Q. Xiao, Microstructure and electrical properties of Mn/Y codoped $Ba_{0.67}Sr_{0.33}TiO_3$ ceramics, Ceramics International 38 (2012) 2785–2791.
[7] Y. Sato, H. Kanai, Y. Yamashita, Grain dielectric dependence of doelectric constant for modified $PbBaZrTiO_3$ ceramic material, Japanese Journal of Applied Physics 33 (1994) 1380–1384.
[8] C. Shen, Q.F. Liu, Q. Liu, Sol–gel synthesis and spark plasma sintering of $Ba_{0.5}Sr_{0.5}TiO_3$, Materials Letters 58 (2004) 2302–2305.
[9] C.L. Mao, X.L. Dong, T. Zeng, Formation and control of mechanism for the preparation of ultra-fine barium strontium titanate powders by the citrate precursor method, Materials Research Bulletin 42 (2007) 1602–1610.
[10] Q. Xu, X.F. Zhang, Y.H. Huang, Sinterability and nonlinear dielectric properties of $Ba_{0.6}Sr_{0.4}TiO_3$ derived from a citrate method, Journal of Alloys and Compounds 485 (2009) L16–L20.
[11] G. Liu, H.L. Guo, P. Yu, Study on intrinsic pyroelectric property of Mn doped BST ceramics, Function Materials 41 (2010) 1053–1055.
[12] Q. Xu, X.F. Zhang, Y.H. Huang, W. Chen, Effect of sintering temperature on structure and nonlinear dielectric properties of$Ba_{0.6}Sr_{0.4}TiO_3$ ceramics prepared by the citrate method, Journal of Physics and Chemistry of Solids 71 (2010) 1550–1556.
[13] J.H. Yoo, W. Gao, Pyroelectric and dielectric bolometer properties of Sr modified $BaTiO_3$ ceramics, Journal of Materials Science 34 (1999) 5361–5369.
[14] G.Z. Zhang, S.L. Jiang, Y.K. Zeng, High pyroelectric properties of porous $Ba_{0.67}Sr_{0.33}TiO_3$ for uncooled infrared detectors, Journal of the American Ceramic Society 92 (2009) 3132–3134.
[15] C.G. Wu, Y.R. Li, J. Zhu, Great enhancement of pyroelectric properties for $Ba_{0.65}Sr_{0.35}TiO_3$ films on pt-substrates by inserting a self-buffered layer, Journal of Applied Physics 105 (2009) 044107.
[16] M.L. Zhao, C.L. Wang, W.L. Zhong, P.L. Zhang, Dielectric and pyroelectric properties of $SrBi_4Ti_4O_{15}$-based ceramics for high-temperature applications, Materials Science and Engineering B B99 (2003) 143–146.